IEEE Open Journal of
Antennas and Propagation

Received 31 March 2022; revised 22 April 2022; accepted 24 April 2022. Date of publication 6 May 2022; date of current version 17 May 2022.

Digital Object Identifier 10.1109/OJAP.2022.3173159

A Novel Cross-Band Decoupled Shared-Aperture Base Station Antenna Array Unit for 5G Mobile Communications

YEJUN HE[1] (Senior Member, IEEE), WEI HUANG[1], ZHOU HE[2], LONG ZHANG[1] (Member, IEEE), XIAOBING GAO[1], AND ZHI ZENG[3] (Member, IEEE)

[1]College of Electronics and Information Engineering, Shenzhen University, Shenzhen 518060, China

[2]Department of Mechanical Engineering, University of Maryland, College Park, MD 20742, USA

[3]Central Research Institute, Sunway Communication Company Ltd., Shenzhen 518125, China

CORRESPONDING AUTHOR: Y. HE (e-mail: heyejun@126.com; yjhe@szu.edu.en)

This work was supported in part by the National Natural Science Foundation of China (NSFC) under Grant 62071306 and Grant 61801299, and in part by the Shenzhen Science and Technology Program under Grant JCYJ20200109113601723, Grant JSGG20210420091805014, Grant JSGG20210802154203011, and Grant GJHZ20180418190529516.

ABSTRACT In this paper, a novel compact, dual-polarized, dual-broadband shared-aperture antenna array unit consisting of one lower-band (LB) element and four upper-band (UB) elements underneath is proposed for 5G mobile communications. L-shaped parasitic branches are introduced in the LB to broaden the bandwidth while reducing the mutual coupling between the LB element and UB elements. Compared with the traditional lower-band dipole, the proposed LB element has far less influence on the electric field of the UB array, thus preserving their radiation patterns. To verify its performance, the antenna array unit is fabricated and experimentally demonstrated to achieve the bandwidth of 32.7% (0.69-0.96 GHz) in the LB and 45.5% (1.7-2.7 GHz) in the UB with a voltage standing wave ratio (VSWR) of lower than 1.5. High port isolation and stable radiation patterns are attained in both the LB and UB as required for dual-band base station antennas.

INDEX TERMS Cross-band decoupling, dual-polarized, interleaved scheme, 5G mobile communications, base station antennas.

I. INTRODUCTION

SINCE the emergence of the first generation of mobile communication in the 1970s, mobile communications technology has been evolving rapidly for meeting the stringent requirements from industries. As more and more frequency bands are being used in mobile communications, one of the major trends of base station antenna development is to achieve dual-band dual-polarization operation and wider bandwidth within each band. However, when combining elements operating at different bands, the mutual cross-band coupling between elements would often lead to the cross-band port isolation distortion, radiation pattern distortion, and impedance mismatch. The mutual coupling problem is an incendiary challenge in dual-band antenna arrays.

Recently, various ways to design dual-polarized, dual-band base station antennas have been proposed. It is the first time for the embedded structure to be proposed in [1]. A dual-band dual-polarized base station antenna using an embedded scheme is proposed in [2], which is composed of four LB dipoles placed vertically around a UB element. In order to suppress a strong mutual coupling caused by this embedded structure, different from the external decoupling network in [3], a method to introduce filtering stubs in the feeding balun is proposed in [4]. In [1] and [5], the metal UB dipole is placed inside the bowl-shaped LB element. Many metal bars are added to ensure the stability of radiation patterns, which increases the complexity of the antenna. For a better grating lobe performance, two LB

elements with different sizes are employed in [6]. Only one UB element is placed in the smaller LB element, while two UB elements are nested in the larger LB element. In [7], a UB-ground-LB stacked structure was used to design antennas operating in 0.69 to 0.96 GHz and 3.5 to 4.9 GHz bands. However, the profile and cost of the antenna are relatively high. A frequency selective surface was introduced by [8] in place of the ground, which resulted in a slightly lower profile height of the LB element. In [9], two subarrays of UB elements are placed on the left and right sides of the LB elements to form the dual-band base station antenna. However, because the high-order modes on the LB are easily excited at the high-frequency band, the effects of mutual coupling can not be ignored, which tends to spoil the port isolation, impedance matching, and the radiation pattern at the high-frequency band. In order to reduce the mutual coupling, the UB and LB elements need to be sufficiently separated and metal walls are added to prevent deterioration of the radiation pattern, which increases the width of the antenna size. Similarly, the side-by-side structure is not conducive to miniaturization [10].

To reduce the width of the antenna array, the researchers try to place the cross-band elements closer by introducing coupling suppression features into the antenna. The interleaved scheme with coupling suppression characteristic is presented. In recent years, methods of suppressing mutual coupling between cross-band elements have been proposed. A dual-polarized LB dipole with an integrated low-pass filter in the balun was proposed in [11], which can suppress the UB (1.69-2.69 GHz and 3.3-3.8 GHz) harmonics. In [12], a spiral choke was used as a low-band radiator, which can also work for scattering suppression. This spiral-choked LB element covering 1.71-2.26 GHz bands and four UB elements covering 3.3-3.7 GHz bands are interlaced to form a dual-band base station antenna array. An LB radiator composed of periodic split-ring resonators is proposed in [13] to reduce the scattering properties of UB. The LB element in [14] based on the wide-angle bandpass frequency selective surface has little effect on the UB radiation pattern. By introducing chokes in the LB radiator, UB scattering currents were significantly suppressed [15]. To reduce the cross-band scattering effect, some methods to improve the LB element radiator have been proposed, such as adding some branches [16] and loading shorted patches [17].

In this paper, an LB element with coupling suppression function is proposed, and it is placed in the middle of the four UB elements to design a dual-band base station antenna. The measured and simulated results show that the presented LB and UB elements operate normally at the 0.69-0.96 GHz and 1.7-2.7 GHz frequency bands, respectively, without affecting each other. The main contributions of this article are as follows.

1) A novel dual-broadband, dual-polarized interleaved shared-aperture base station antenna array unit is designed. The operating bandwidth exceeds most of the existing dual-band dual-polarized base station antennas.

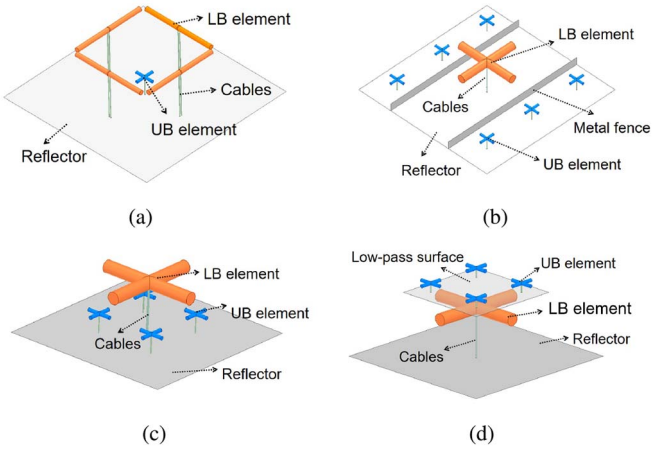

FIGURE 1. Main structures of dual-band antenna array. (a) Embedded scheme. (b) Side-by-side scheme. (c) Interleaved scheme. (d) Stacked scheme.

2) An unblocked LB radiator is proposed to reduce the blocking of UB radiation waves. By loading the L-shaped branches, the UB-induced current on the LB radiator is suppressed. A low-pass filtering balun is used to excite the LB radiator, and an L-shaped stub is introduced on the Γ-shaped feeding line to improve cross-band ports isolation.

3) Integrating the LB element into the 2×2 UB array, the proposed LB element has a negligible effect on the UB electric field. Thus, the preservation of the UB radiation pattern is achieved.

II. ANTENNA ELEMENTS DESIGN

A. PRELIMINARY OF DUAL-BAND ANTENNA STRUCTURES

The approaches to designing a dual-band antenna by combining the upper and lower band elements mainly rely on the embedded scheme, side-by-side scheme, interleaved scheme, and stacked scheme, as shown in Fig. 1. The embedded scheme shown in Fig. 1(a) has high space utilization and can greatly reduce the size. But it will lead to aggravation of cross-band coupling. Compared with the traditional side-by-side structure shown in Fig. 1(b), the interleaved structure in Fig. 1(c) can reduce the size of the antenna. The interleaved structure has a lower cost in mass production compared with a stacked structure which consists of UB element, LB-pass surface, and LB element, as shown in Fig. 1(d). Therefore, the interleaved structure is a relatively ideal dual-band antenna array scheme.

B. UPPER-BAND ELEMENT

Fig. 2 shows the structure of the UB element, which mainly consists of two perpendicular die-cast dipoles supported by a balun connector, two Γ-shaped probes, a parasitic patch, and a reflector. A Y-shaped branch is added to the square loop dipoles to extend the bandwidth. As illustrated in Fig. 2(a), two coaxial cables are used to excite the two Γ-shaped probes at Port 1 and Port 2. The outer conductor of the coaxial cable connects with the corresponding balun

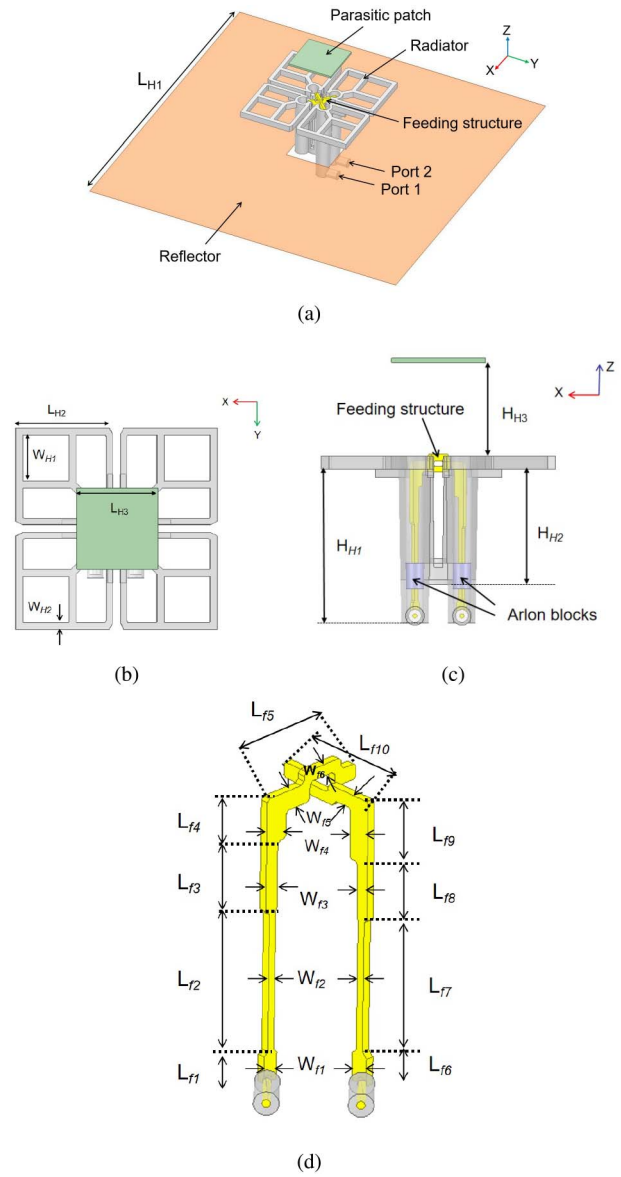

FIGURE 2. Configuration of the proposed UB element. (a) 3D view. (b) Top view. (c) Side view. (d) The feeding structure.

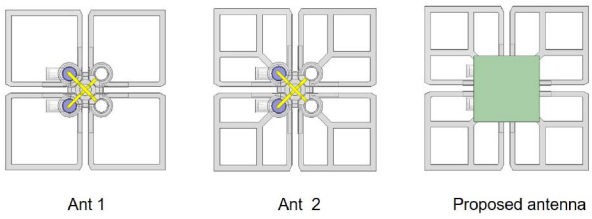

FIGURE 3. Top view of the reference antennas and the proposed UB antenna.

TABLE 1. Dimensions of the proposed UB element.

Parameter	Value	Parameter	Value	Parameter	Value
L_{H1}	160	L_{H2}	25.5	L_{H3}	22
W_{H1}	12.5	W_{H2}	2	H_{H1}	36
H_{H2}	26	H_{H3}	22	L_{f1}	4
L_{f2}	17.7	L_{f3}	8.7	L_{f4}	6.4
L_{f5}	14.3	L_{f6}	4.2	L_{f7}	16.7
L_{f8}	7.1	L_{f9}	8.3	L_{f10}	14
W_{f1}	2	W_{f2}	1	W_{f3}	1.8
W_{f4}	3	W_{f5}	2.5	W_{f6}	1.5

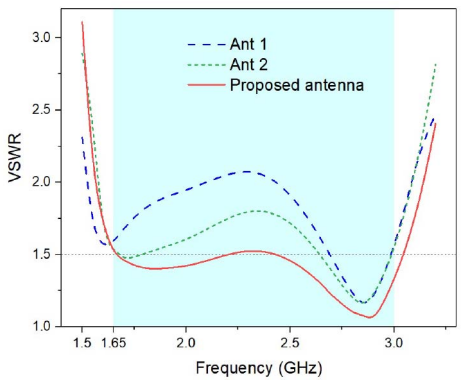

FIGURE 4. Simulated VSWR of the reference antennas and the proposed UB antenna.

connector of one square loop, the inner conductor connects with Γ-shaped probe and this probe connects with the other square loop of the same dipole at the other end. Fig. 2(b) is the top view of the square loop dipoles. As shown, dipoles 1 and 2 produce $+45°$ and $-45°$ polarizations, respectively. Fig. 2(c) is the side view of the proposed UB element, where Arlon blocks are selected as PTFE AD270 to fix Γ-Shaped feed probes. Fig. 2(d) shows the construction of the feeding probe. This probe works as a quarter-wave impedance transformer. The input impedance of the antenna can be adjusted by tuning the line width of this structure, so as to achieve better impedance matching. A parasitic metal patch is suspended above the dipole to extend the bandwidth and enhance impedance matching. The antenna is simulated and optimized in HFSS, and the optimized parameters are shown in Table 1.

In order to better illustrate the design mechanism of the UB element, the simulated results of the proposed UB element and two reference antennas are compared and analyzed. A top view of the reference antennas and the proposed UB antenna are shown in Fig. 3. Ant 1 is a simple square loop structure without a parasitic patch and Y-shaped branches inside the loop. Ant 2 adds Y-shaped branches in the loops of the basic Ant 1 structure. The comparison of results of the simulated VSWR of the three antennas is shown in Fig. 4.

It can be seen that the introduction of Y-shaped branches and a parasitic patch makes the first resonant point of the antenna move to the high frequency, while the second resonant point remains unchanged. The maximum value of VSWR of Ant 1 within 1.7-2.7 GHz is about 2.2. With the addition of Y-shaped branches, the maximum VSWR of

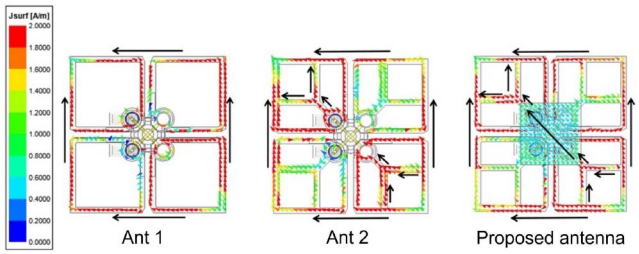

FIGURE 5. Comparison of antennas' surface current distributions.

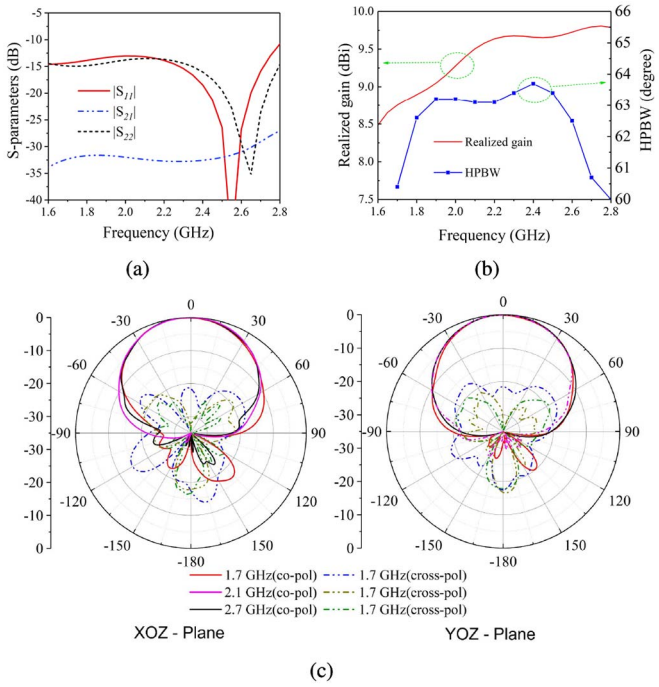

FIGURE 6. Simulated (a) *S* parameters, (b) Realized gain and HPBW, and (c) Radiation patterns of the UB element.

the antenna decreases to 1.75. The addition of the parasitic patch can further enhance the antenna impedance matching. With the addition of the parasitic patch, the VSWR of the antenna drops below 1.5 within the operating band.

Fig. 5 shows the surface current distribution of the reference antennas and the proposed UB antenna operating at 2.1 GHz. It can be seen that the Y-shaped branches can excite the induced current in the same direction as the dipole surface current, which enhances the radiation of the current in this polarization. The parasitic patch is mainly used to improve the impedance matching, and then enhance the bandwidth.

Fig. 6(a) shows the *S*-parameters of the proposed UB antenna. This antenna element can operate at 1.7-2.7 GHz band with $|S_{11}| < -14$ dB and $|S_{12}| < -30$ dB. In Fig. 6(b), the average gain of 9.2 dBi and the HPBW of 60°−63.7° of the UB antenna are obtained. The radiation patterns are presented in Fig. 6(c). It shows that the UB antenna has stable radiation performance at the high-frequency band.

TABLE 2. Dimensions of the proposed LB element.

Parameter	Value	Parameter	Value	Parameter	Value
H_{l1}	80	H_{l2}	27	W_{l1}	45
W_{l2}	2	L_{l1}	250	L_{l2}	116
L_{l3}	38	L_{l4}	13.8	L_{l5}	6.2
L_{l6}	10.4	L_{l7}	5.4	L_{l8}	16
L_{l9}	6	L_{l10}	39	L_{l11}	24
L_{b1}	79.2	L_{b2}	24.5	L_{b3}	24.6
L_{b4}	23.35	L_{b5}	14.5	L_{b6}	12.45
L_{b7}	5	L_{b8}	16	L_{b9}	15.4
L_{b10}	25.6	L_{b11}	24.15	L_{b12}	14.5
L_{b13}	11.25	W_{b1}	4	W_{b2}	5.3
W_{b3}	1.5	W_{b4}	1.1	W_{b5}	2
W_{b6}	9.7	W_{b7}	3		

C. LOWER-BAND ELEMENT

Fig. 7 shows the configuration of the LB element. As shown, the LB element is mainly composed of two perpendicular square loop dipoles with L-shaped branches, two pairs of baluns and a reflector. The dipoles are printed on the top side of the FR4 substrate, and 6 L-shaped branches are added inside the square loop, which can be used to widen the bandwidth and reduce the UB radiation distortion. In order to clearly illustrate the role of L-shaped branches, we divide the L-shaped branches into two parts, called branches 1 and 2 as shown in Fig. 7(b). The geometry of the baluns is detailed in Fig. 7(d). Two coaxial cables are used to excite the two baluns at the feed points. To construct the baluns, two vertically placed substrates with permittivity of 3, loss tangent of 0.003 and thickness of 1.52 mm are set perpendicular to each other. A microstrip line and a slot line are printed on the front and the back sides of the substrate, respectively. The grooves of the two substrates are staggered to each other for easy fixation. The balun proposed in this paper follows the basic design principles [18], [19], [20]. The difference is that an L-shaped stub is added on a Γ-shape microstrip line, connecting with the rear of the substrate by metal via, which is used to enhance the cross-band ports isolation.

To better explain the role of the branches, three reference antennas are proposed and simulated. As shown in Fig. 8, they are named LBant 1, LBant 2, and LBant 3. LBant 1 is a square loop dipole antenna without any branches. LBant 2 adds branch 1 on the basis of LBant 1, and LBant 3 adds branch 2 on the basis of LBant 2. The proposed LB antenna adds coupling lines on the back of LBant 3.

Fig. 9 shows the induced current distribution of LBant 2 and LBant 3 at 2.5 GHz when the UB element is excited. In

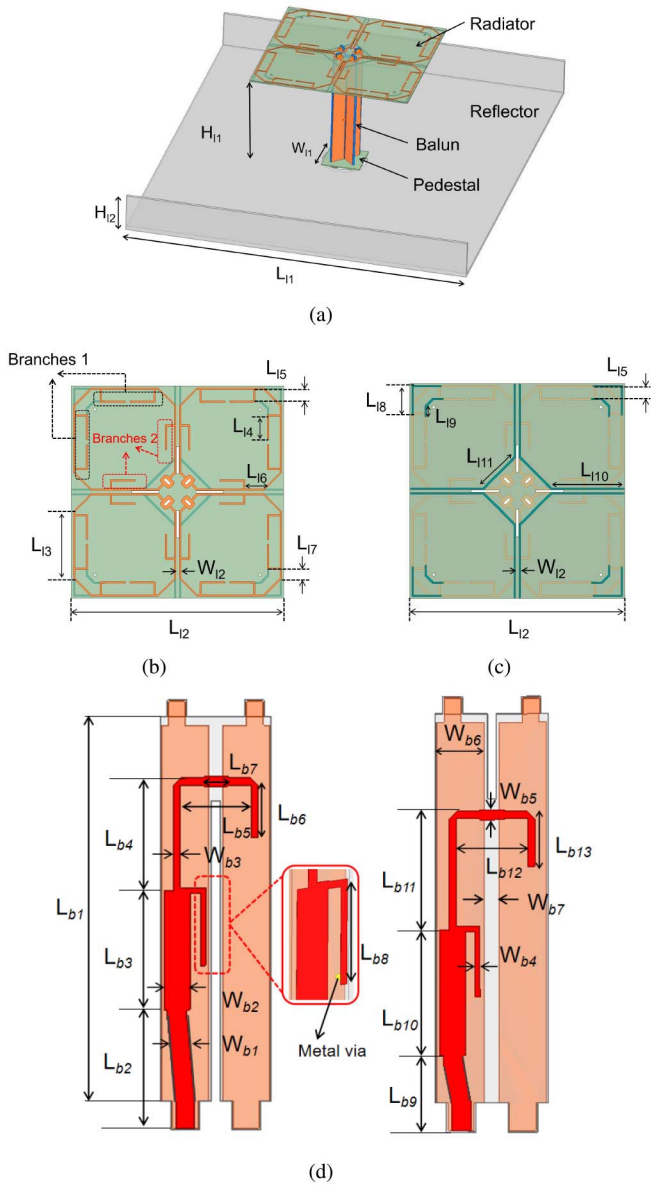

FIGURE 7. Configuration of the LB element. (a) 3D view. (b) Top view and (c) bottom view of the radiator. (d) Structure of the baluns.

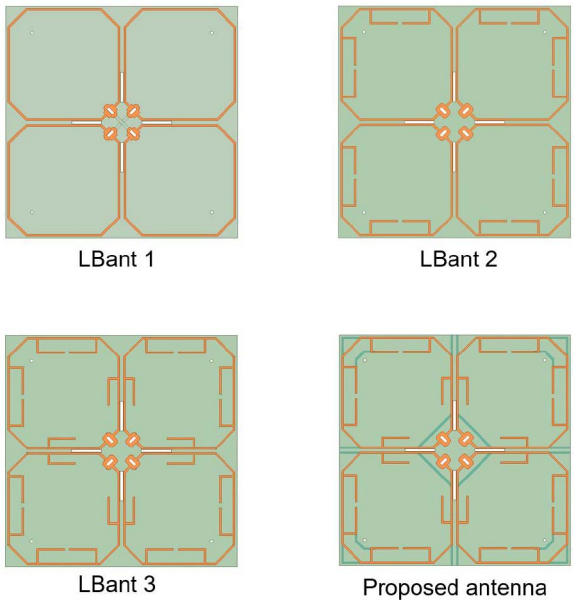

FIGURE 8. Top view of the reference antennas and the proposed LB antenna.

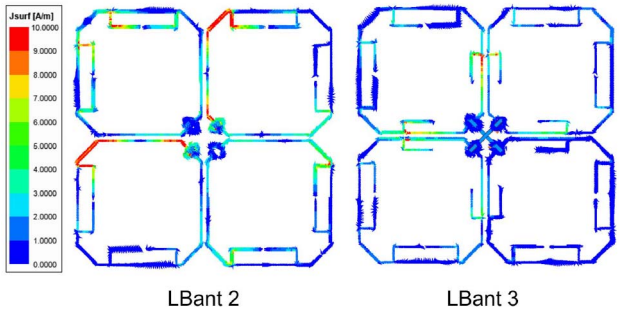

FIGURE 9. The surface current distribution of LBant 2 and LBant 3 at 2.5 GHz.

LBant 2, strong currents are induced and distributed on the chamfer edge and branch 1, which will excite new electromagnetic waves and interfere with the electromagnetic waves radiated by the UB element, resulting in cross-band scattering and blockage effect. For the LBant 3, The induced current is significantly reduced. In this case, the induced current on the LB radiator is concentrated on the branch 2 far from the UB unit, while the current on the branch 1 and chamfer edge close to the UB unit is greatly suppressed, resulting in radiation cancelation, thus greatly reducing the influence on the UB radiation. This shows that the branch 2 can reduce the blockage effect on the UB radiation, keeping the UB radiation pattern stable. In addition, adding coupling lines on the back of the LBant 3 can slightly reduce the VSWR of the UB antennas when forming an array. It is helpful to both UB and LB antennas' cross-polarization suppression as well.

In order to reduce the blockage effect of LB element on the radiation of UB array, the presented antenna with branches and coupled lines replaces the traditional low-band dipole LBant 1. For verification, Fig. 10 compares the distribution of E-field in the XOZ-plane in three cases: case (1) UB array working alone; case (2) UB array with LBant 1; case (3) UB array with the proposed LB element. Obviously, when LBant 1 is placed above the UB array, it blocks the propagation of the electromagnetic wave from the UB array. Therefore, the electric field distribution of the UB array is greatly disturbed. Fortunately, this blockage effect is significantly reduced in case (3). It can be seen that the proposed LB element is almost transparent to the UB array, and the electric field is also restored as in free space. Fig. 10(b) shows the XOZ-plane radiation pattern in three cases within the operating band, which is consistent with the situation presented in Fig. 10(a). Using LBant 1 will make the main beam of the UB radiation pattern sag or tilt, while the

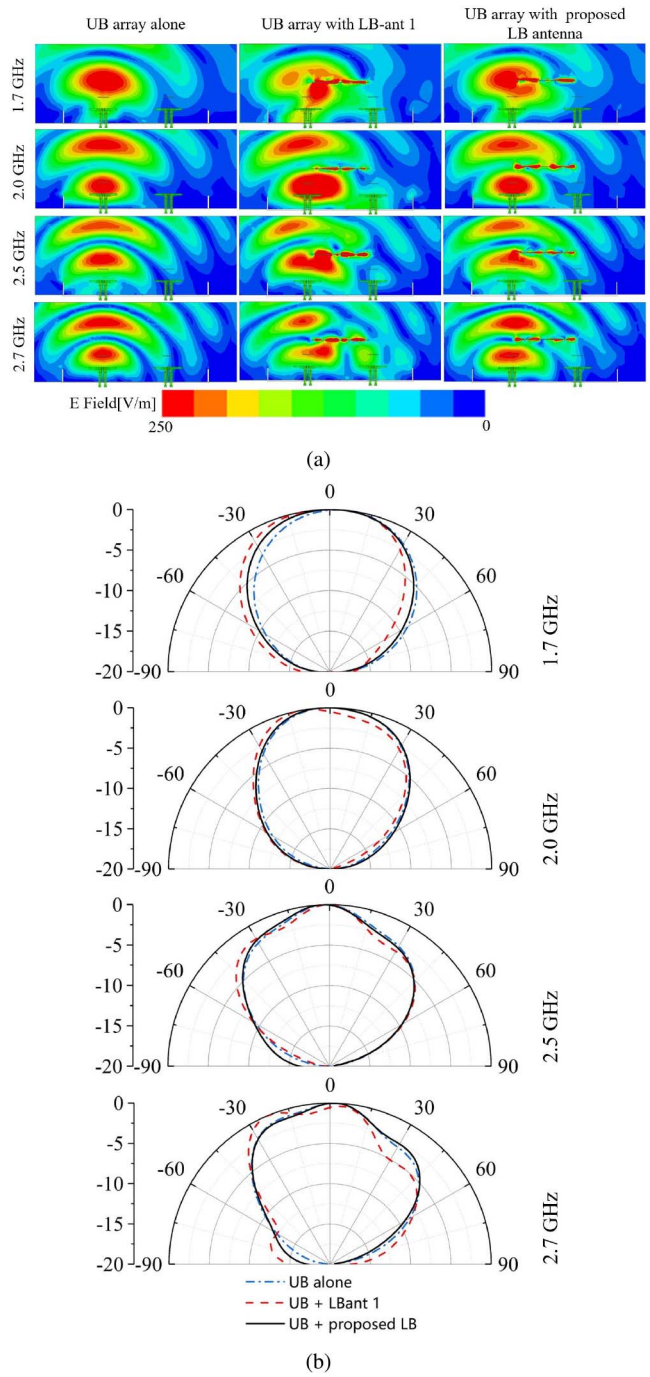

FIGURE 10. Comparison of (a) E-field cuts and, (b) Normalized UB radiation patterns in the XOZ-plane in the cases of i) UB array alone, ii) UB array with LBant 1, and iii) UB array with the proposed LB element.

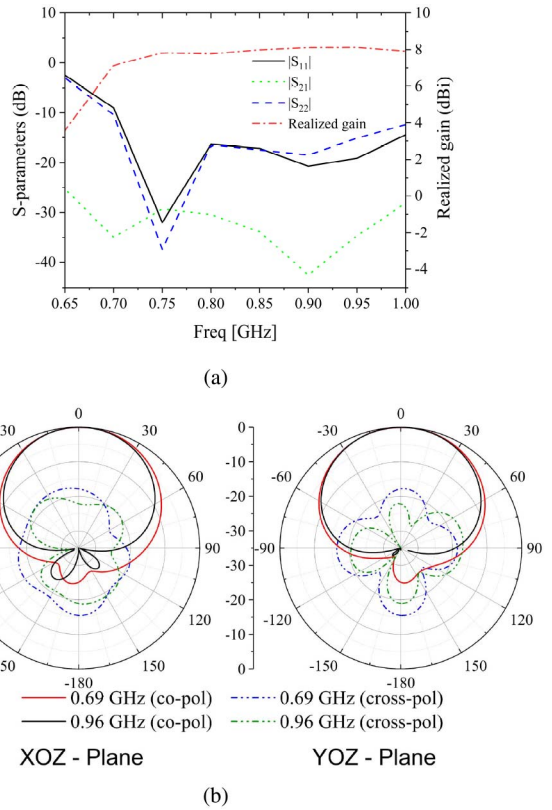

FIGURE 11. Simulated (a) *S* parameters and Realized gain, and (b) Radiation patterns of the LB element.

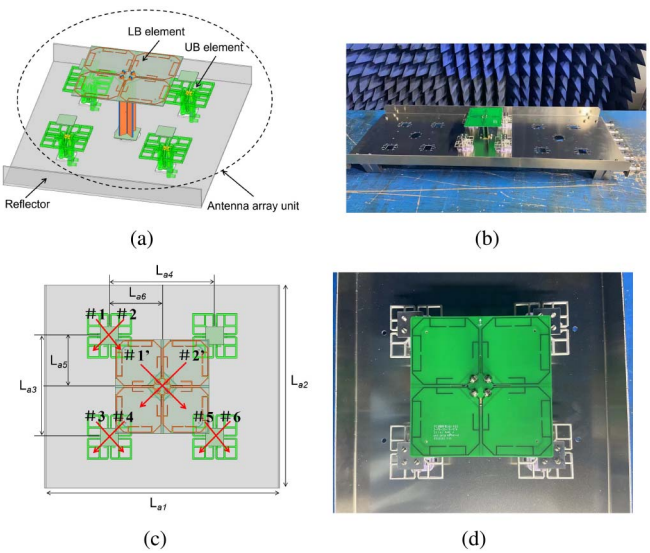

FIGURE 12. Configuration of the dual-band antenna array unit. (a) 3D view of simulation model, (b) 3D view of prototype, (c) Top view of simulation model, (d) Top view of prototype.

proposed LB element has almost negligible influence on the radiation pattern of the UB array.

The simulated *S* parameters of the LB element are illustrated in Fig. 11(a). The operating band is 0.72-0.96 GHz with $|S_{11}|$ of less than -15dB. $|S_{12}|$ is less than -25 dB, indicating that the LB element has high isolation between two polarization ports. The simulated gains of the proposed LB antenna are shown in Fig. 11(a) as well. As shown, the average simulated gain in the operating band is about 7.8 dBi. In addition, the XOZ-plane and YOZ-plane radiation patterns of the LB element at 0.69 GHz, and 0.96 GHz are shown in Fig. 11(b). Due to the symmetry of the antenna structure, only the radiation patterns for $+45°$ polarization

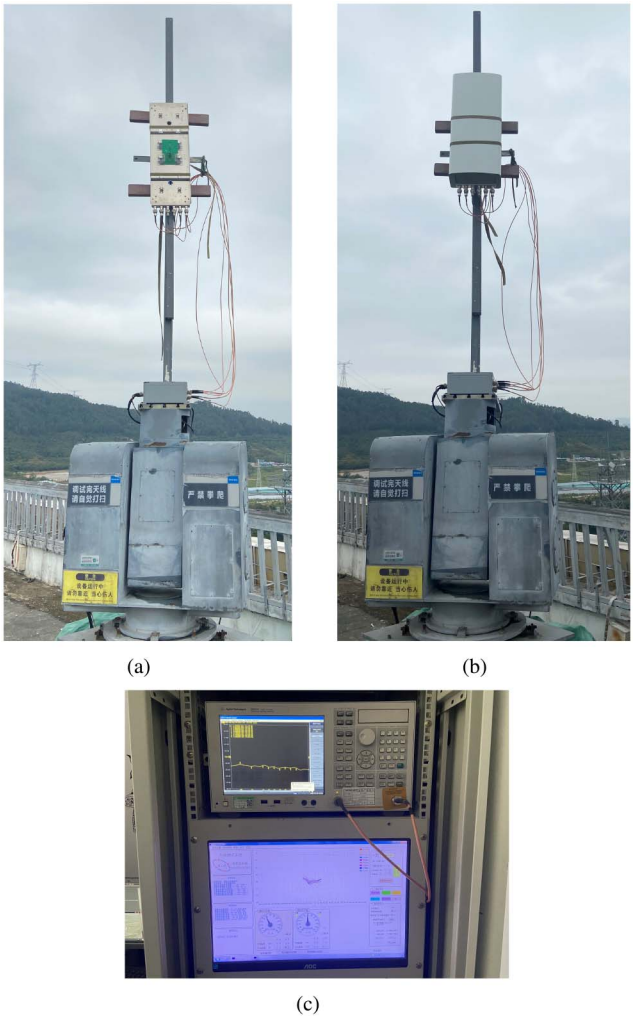

FIGURE 13. Measured scenario of the proposed base station antenna array unit: (a) the rotating pole with antenna array unit (without radome) on the roof of building, (b) the rotating pole with antenna array unit (with radome) on the roof of building, (c) far-field antennas measurement system in the room of the building.

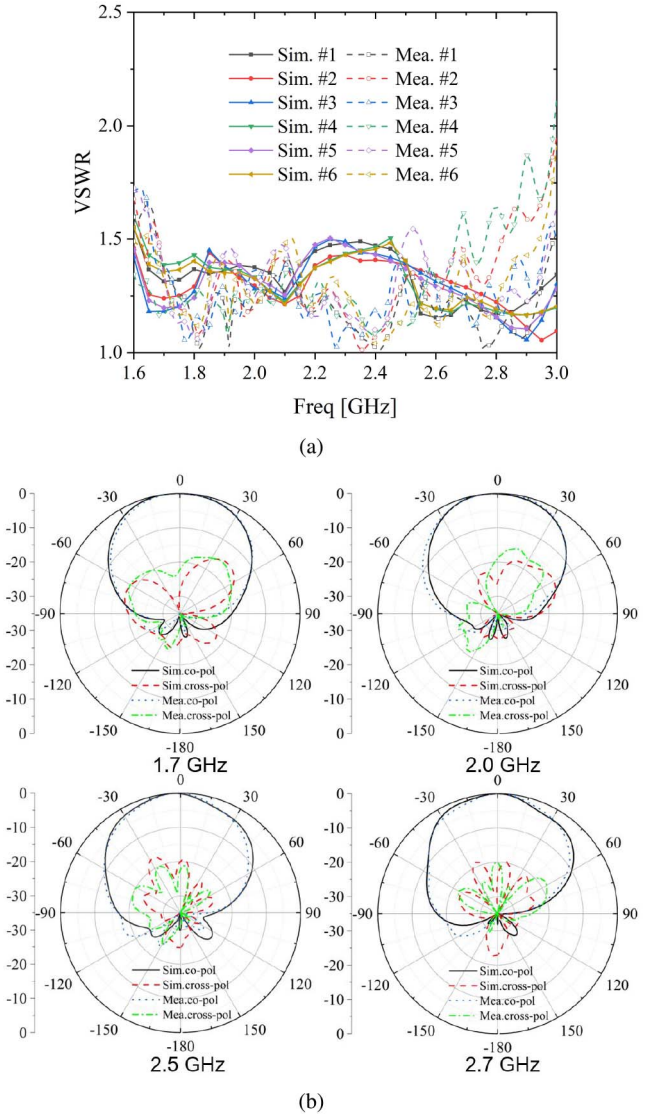

FIGURE 14. Simulated and measured (a) VSWR and (b) Radiation patterns (XOZ-plane, port #1 and port #3 are excited) of the UB array.

are presented here. HPBWs are in a range of 60°-70° in LB. Obviously, the proposed LB antenna element has a wide operating bandwidth, stable radiation pattern in-band and transparent transmission characteristics at high frequencies.

III. ANTENNA ARRAY UNIT

Based on the above analysis, the simulation model of a base station antenna array unit composed of 1 LB element and 4 UB elements is designed, as shown in Fig. 12 (a), (c). To validate the design method, the prototype of the antenna array unit shown in Fig. 12 (b), (d) is fabricated. The measured scenario is shown in Fig. 13.

Considering the symmetry of the proposed antenna array unit, for brevity, six UB ports (#1-#6) and two LB ports (#1' and #2') marked in Fig. 12(c) are mainly analyzed. The measured VSWR of #1-#6 ports is given in Fig. 14(a). For comparison, the simulated VSWR is also displayed. As the results show, the simulated VSWR of the proposed UB array is less than 1.5 in the frequency range of 1.6-3 GHz, while the measured impedance bandwidth is 45.5% (1.7-2.7 GHz). Fig. 14(b) presents the simulated and measured XOZ-plane radiation patterns of the UB array (port #1 and port #3 are excited) at 1.7 GHz, 2.0 GHz, 2.5 GHz, and 2.7 GHz. Obviously, the measured radiation patterns are in good agreement with the simulated ones. However, the symmetry of the radiation patterns at 2.5 GHz and 2.7 GHz are slightly weakened. This is resulting from the mutual coupling between the UB elements. The simulated and measured cross-polarization discriminations (XPDs) are greater than 20 dB and 19 dB, respectively.

As illustrated in Fig. 15(a), the measured VSWR of the proposed LB element is in good agreement with the simulated one. The simulated VSWR of the LB element is less than 1.5 in the frequency range of 0.7-0.96 GHz, while the

TABLE 3. Comparison between existing dual-band dual-polarized antennas and this work.

Ref	Upper-band antenna				Lower-band antenna			
	Bandwidth	Gain(dBi)	HPBW	Element Size(λ_U^3)	Bandwidth	Gain(dBi)	HPBW	Element Size(λ_L^3)
[1]	23.7%(VSWR<1.5)	18±1	62°±4°	0.35×0.35×0.25	15.7%(VSWR<1.5)	14±1	69.5°±1.7°	0.38×0.38×0.22
[2]	55%(VSWR<2)	14.5±1.2	79°±5°	0.35×0.35×0.25	23.4%(VSWR<2)	14.4±0.6	60.8°±3.7°	0.49×0.49×0.22
[8]	33.3%(VSWR<2)	8.1±1	75°±20°	0.52×0.52×0.25	32.7%(VSWR<2)	8.8±1	58.5°±6.5°	0.69×0.69×0.12
[12]	11.4%(VSWR<1.5)	10.9±0.9	66.5°±3.5°	N/A	28.3%(VSWR<1.5)	7±1	65°±5°	N/A
[13]	24%(VSWR<2)	12.8±1.2	100°±13°	0.41×0.41×0.18	32.7%(VSWR<2)	7.7±0.4	64.5°±3°	0.33×0.33×0.25
[14]	14.1%(VSWR<1.5)	7.2±0.9	88°±4°	0.38×0.38×0.24	40%(VSWR<1.5)	8.6±1.3	62.5°±3.5°	0.31×0.31×0.19
[15]	28.6%(VSWR<2)	11±1	65°±5°	N/A	19.7%(VSWR<2)	6.5±0.5	69.5°±4°	0.42×0.42×0.3
[17]	14.1%(VSWR<2)	10.69(avg.)	67.5°±1.5°	0.53×0.71×0.39	23.8%(VSWR<2)	7.9(avg.)	61.5°±7.5°	N/A
[21]	23.7%(VSWR<2)	10.1±0.5	72.5°±9.5°	0.42×0.42×0.3	23.7%(VSWR<2)	7.5±0.2	61.5°±7.5°	0.46×0.46×0.26
This work	45.5%(VSWR<1.5)	11.3±0.7	60°±6.5°	0.37×0.37×0.25	32.7%(VSWR<1.5)	7.6±0.6	76°±8°	0.32×0.32×0.22

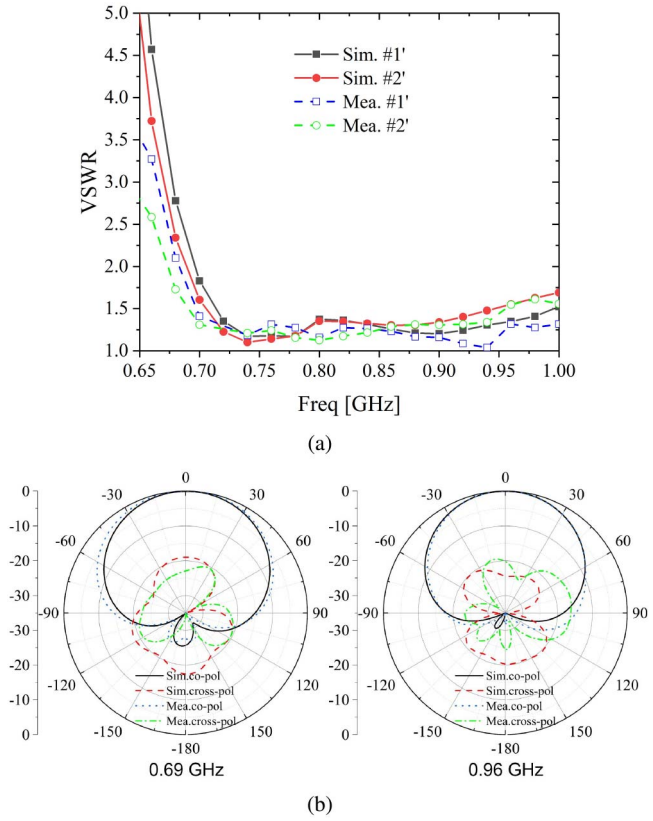

FIGURE 15. Simulated and measured (a) VSWR and (b) Radiation patterns (XOZ-plane, port #1' is excited) of the LB element.

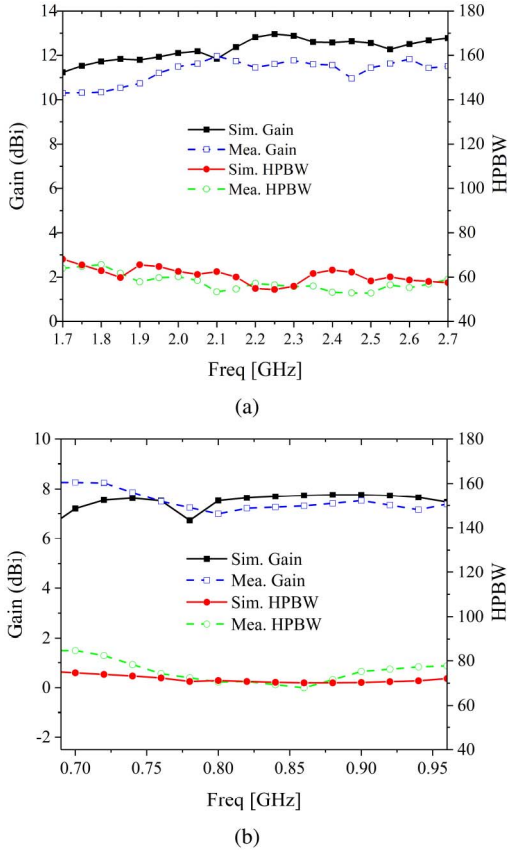

FIGURE 16. Simulated and measured gain and HPBW. (a) UB array (port #1 and port #3 are excited). (b) LB element (port #1' is excited).

measured 1.5-VSWR band is from 0.69 GHz to 0.96 GHz. The radiation patterns of the LB element (port #1' is excited) at 0.69 GHz and 0.96 GHz are given in Fig. 15(b). The measured radiation patterns are as symmetrical and stable as the simulated ones in the lower band. The simulated XPD of the proposed LB element is 19 dB, and the measured XPD reaches 20 dB.

The gain and half-power beamwidth at the upper and lower bands of the proposed antenna unit are depicted in Fig. 16 (a) and (b), respectively. The measured results show that the gain of the UB array is 11.3±0.7 dBi, and the HPBW is 60°±6.5°; the gain of the LB array is 7.6±0.6 dBi, and the HPBW is in the range of 76°±8°. Figs. 17 and 18 reveal the simulated and measured isolation coefficients of the proposed antenna

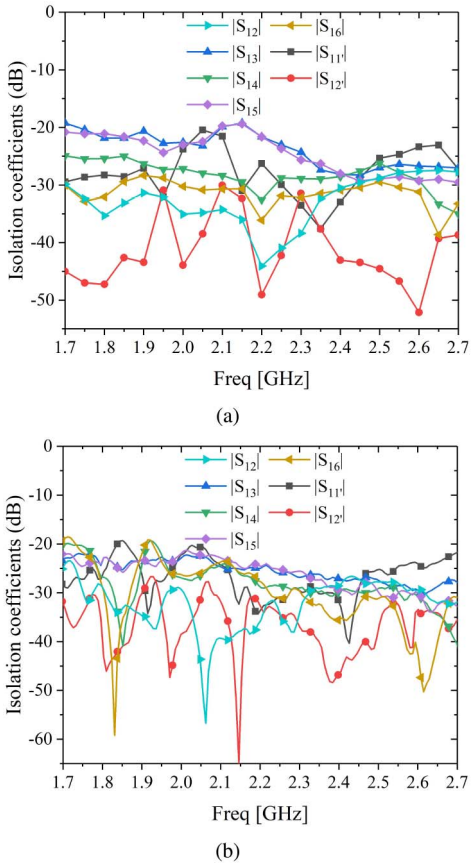

FIGURE 17. (a) Simulated and (b) measured isolation coefficients in upper band.

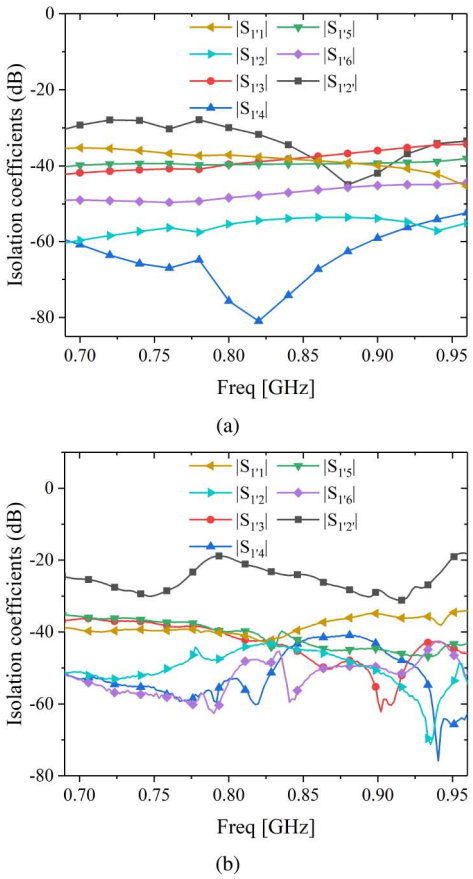

FIGURE 18. (a) Simulated and (b) measured isolation coefficients in lower band.

array unit operating in the upper and lower bands, respectively. It can be seen from Fig. 17 that, at the 1.7-2.7 GHz band, the measured isolation coefficients of the UB element and any other antenna element are less than −19 dB. The isolation coefficients of the LB element are given in Fig. 18. The simulated and measured isolation coefficients of the $|S_{1'2'}|$ ports are less than −23 dB and −19 dB, respectively, and the processing error and the interference of the coaxial feeder are the main reasons for this. The isolation between the LB element and any UB array element is lower than −33 dB, which verifies the cross-band coupling suppression capability of the proposed antenna array unit. Table 3 summarizes the performance comparison of existing dual-band dual-polarized antennas, where λ_U and λ_L represent the free-space wavelength of the center frequency of upper and lower bands, respectively. It can be seen that the proposed LB element has a relatively small size. Different from other reference antennas, the proposed antenna unit exhibits a satisfactory bandwidth performance in both upper and lower bands.

IV. CONCLUSION

In this paper, a novel dual-polarized dual-broadband base station antenna array unit with cross-band decoupling feature is designed. In the upper band, the radiation cancels out by generating current on L-shaped branches which is opposite to that on the square dipole, so as to reduce the coupling and the deterioration of high-frequency radiation patterns. The simulated and measured results show that the antenna array unit has good impedance matching, high polarization isolation and cross-band isolation, stable radiation pattern and cross-band coupling suppression in the lower bands of 0.69 to 0.96 GHz and the upper bands of 1.7-2.7 GHz, thus the presented antenna array unit can be used as a dual-band shared-aperture base station antenna array for 5G mobile communications. Although the proposed base station antenna array unit only includes one LB element and four UB elements, other array units can also be studied by selecting various combinations of elements so that milti-band or all-spectrum-access base station antennas can be reconfigured in terms of frequency, bandwidth, and radiation pattern.

REFERENCES

[1] Y. He, Z. Pan, X. Cheng, Y. He, J. Qiao, and M. M. Tentzeris, "A novel dual-band, dual-polarized, miniaturized and low-profile base station antenna," *IEEE Trans. Antennas Propag.*, vol. 63, no. 12, pp. 5399–5408, Dec. 2015.

[2] H. Huang, Y. Liu, and S. Gong, "A novel dual-broadband and dual-polarized antenna for 2G/3G/LTE base stations," *IEEE Trans. Antennas Propag.*, vol. 64, no. 9, pp. 4113–4118, Sep. 2016.
[3] L. Zhao, K.-W. Qian, and K.-L. Wu, "A cascaded coupled resonator decoupling network for mitigating interference between two radios in adjacent frequency bands," *IEEE Trans. Microw. Theory Techn.*, vol. 62, no. 11, pp. 2680–2688, Nov. 2014.
[4] Y. Liu, S. Wang, N. Li, J.-B. Wang, and J. Zhao, "A compact dual-band dual-polarized antenna with filtering structures for sub-6 GHz base station applications," *IEEE Antennas Wireless Propag. Lett.*, vol. 17, pp. 1764–1768, 2018.
[5] R. Wu and Q.-X. Chu, "A compact, dual-polarized multiband array for 2G/3G/4G base stations," *IEEE Trans. Antennas Propag.*, vol. 67, no. 4, pp. 2298–2304, Apr. 2019.
[6] F. Jia, S. Liao, and Q. Xue, "A dual-band dual-polarized antenna array arrangement and its application for base station antennas," *IEEE Antennas Wireless Propag. Lett.*, vol. 19, pp. 972–976, 2020.
[7] Y. Chen, J. Zhao, and S. Yang, "A novel stacked antenna configuration and its applications in dual-band shared-aperture base station antenna array designs," *IEEE Trans. Antennas Propag.*, vol. 67, no. 12, pp. 7234–7241, Dec. 2019.
[8] Y. Zhu, Y. Chen, and S. Yang, "Decoupling and low-profile design of dual-band dual-polarized base station antennas using frequency-selective surface," *IEEE Trans. Antennas Propag.*, vol. 67, no. 8, pp. 5272–5281, Aug. 2019.
[9] Y. He, Y. Yue, L. Zhang, and Z. N. Chen, "A dual-broadband dual-polarized directional antenna for all-spectrum access base station applications," *IEEE Trans. Antennas Propag.*, vol. 69, no. 4, pp. 1874–1884, Apr. 2021.
[10] Y. Zhang, X. Y. Zhang, L.-H. Ye, and Y.-M. Pan, "Dual-band base station array using filtering antenna elements for mutual coupling suppression," *IEEE Trans. Antennas Propag.*, vol. 64, no. 8, pp. 3423–3430, Aug. 2016.
[11] Q.-X. Chu, Y.-L. Chang, and J.-P. Li, "Crisscross-shaped ± 45° dual-polarized antenna with enhanced bandwidth for base stations," *IEEE Trans. Antennas Propag.*, vol. 69, no. 4, pp. 2341–2346, Apr. 2021.
[12] H.-H. Sun, H. Zhu, C. Ding, B. Jones, and Y. J. Guo, "Scattering suppression in a 4G and 5G base station antenna array using spiral chokes," *IEEE Antennas Wireless Propag. Lett.*, vol. 19, pp. 1818–1822, 2020.
[13] S. J. Yang, Y. Yang, and X. Y. Zhang, "Low scattering element-based aperture-shared array for multiband base stations," *IEEE Trans. Antennas Propag.*, vol. 69, no. 12, pp. 8315–8324, Dec. 2021.
[14] D. He, Q. Yu, Y. Chen, and S. Yang, "Dual-band shared-aperture base station antenna array with electromagnetic transparent antenna elements," *IEEE Trans. Antennas Propag.*, vol. 69, no. 9, pp. 5596–5606, Sep. 2021.
[15] H.-H. Sun, C. Ding, H. Zhu, B. Jones, and Y. J. Guo, "Suppression of cross-band scattering in multiband antenna arrays," *IEEE Trans. Antennas Propag.*, vol. 67, no. 4, pp. 2379–2389, Apr. 2019.
[16] X. W. Dai, D. L. Mi, H. Hong, S. Y. Lin, and G. Q. Luo, "Dual-polarized antenna with suppression of cross-band scattering in multiband array," *IEEE Antennas Wireless Propag. Lett.*, vol. 20, pp. 1592–1595, 2021.
[17] S. J. Yang, R. Ma, and X. Y. Zhang, "Self-decoupled dual-band dual-polarized aperture-shared antenna array," *IEEE Trans. Antennas Propag.*, early access, Dec. 29, 2021, doi: 10.1109/TAP.2021.3137531.
[18] L. H. Ye, X. Y. Zhang, Y. Gao, and Q. Xue, "Wideband dual-polarized four-folded-dipole antenna array with stable radiation pattern for base-station applications," *IEEE Trans. Antennas Propag.*, vol. 68, no. 6, pp. 4428–4436, Jun. 2020.
[19] W. K. Roberts, "A new wide-band balun," *Proc. IRE*, vol. 45, no. 12, pp. 1628–1631, Dec. 1957.
[20] C. Ding, B. Jones, Y. J. Guo, and P.-Y. Qin, "Wideband matching of full-wavelength dipole with reflector for base station," *IEEE Trans. Antennas Propag.*, vol. 65, no. 10, pp. 5571–5576, Oct. 2017.
[21] Y.-L. Chang and Q.-X. Chu, "Suppression of cross-band coupling interference in tri-band shared-aperture base station antenna," *IEEE Trans. Antennas Propag.*, early access, Jan. 5, 2022, doi: 10.1109/TAP.2021.3138531.

YEJUN HE (Senior Member, IEEE) received the Ph.D. degree in information and communication engineering from the Huazhong University of Science and Technology, Wuhan, China, in 2005.

From 2005 to 2006, he was a Research Associate with the Department of Electronic and Information Engineering, Hong Kong Polytechnic University, Hong Kong. From 2006 to 2007, he was a Research Associate with the Department of Electronic Engineering, Faculty of Engineering, Chinese University of Hong Kong, Hong Kong. In 2012, he was a Visiting Professor with the Department of Electrical and Computer Engineering, University of Waterloo, Waterloo, ON, Canada. From 2013 to 2015, he was an Advanced Visiting Scholar (Visiting Professor) with the School of Electrical and Computer Engineering, Georgia Institute of Technology, Atlanta, GA, USA. Since 2011, he has been a Full Professor with the College of Electronics and Information Engineering, Shenzhen University, Shenzhen, China, where he is the Director of Guangdong Engineering Research Center of Base Station Antennas and Propagation and the Director of Shenzhen Key Laboratory of Antennas and Propagation, Shenzhen. He was selected as Pengcheng Scholar Distinguished Professor, Shenzhen, and Minjiang Scholar Chair Professor of Fujian Province. He has authored or coauthored more than 230 referred journal and conference papers, 7 books (chapters) and holds about 20 patents. His research interests include wireless communications, antennas, and radio frequency. He received the Shenzhen Science and Technology Progress Award and the Guangdong Provincial Science and Technology Progress Award in 2017 and 2018, respectively. He was also a recipient of the Shenzhen Overseas High-Caliber Personnel Level B ("Peacock Plan Award" B) and Shenzhen High-Level Professional Talent (Local Leading Talent). He has served as a Reviewer for various journals, such as the IEEE TRANSACTIONS ON VEHICULAR TECHNOLOGY, the IEEE TRANSACTIONS ON COMMUNICATIONS, the IEEE TRANSACTIONS ON INDUSTRIAL ELECTRONICS, the IEEE TRANSACTIONS ON ANTENNAS AND PROPAGATION, the IEEE WIRELESS COMMUNICATIONS, the IEEE COMMUNICATIONS LETTERS, the *International Journal of Communication Systems*, *Wireless Communications and Mobile Computing*, and *Wireless Personal Communications*. He is the Chair of IEEE Antennas and Propagation Society-Shenzhen Chapter. He has also served as a Technical Program Committee Member or a Session Chair for various conferences, including the IEEE Global Telecommunications Conference, the IEEE International Conference on Communications, the IEEE Wireless Communication Networking Conference, and the IEEE Vehicular Technology Conference. He served as the TPC Chair for IEEE ComComAp 2021, the General Chair for IEEE ComComAp 2019, and the Organizing Committee Vice Chair for the International Conference on Communications and Mobile Computing (CMC 2010). He was selected as a board member of IEEE wireless and optical communications conference (WOCC) and is serving as the TPC Co-Chair for WOCC 2022. He is the Principal Investigator for over 30 current or finished research projects, including the National Natural Science Foundation of China, the Science and Technology Program of Guangdong Province, and the Science and Technology Program of Shenzhen City. He is a Fellow of IET and a Senior Member of the China Institute of Communications and the China Institute of Electronics. He is serving as an Associate Editor for IEEE TRANSACTIONS ON ANTENNAS AND PROPAGATION, *IEEE Antennas and Propagation Magazine*, IEEE NETWORK, *International Journal of Communication Systems*, *China Communications*, as well as *Wireless Communications and Mobile Computing*.

WEI HUANG is currently pursing the master's degree in electronics and communication engineering from Shenzhen University, Shenzhen, China. His research interests include base station antennas and radio frequency.

ZHOU HE is currently pursing the Ph.D. degree in mechanical engineering with the University of Maryland at College Park, College Park, USA. His research interests include wireless communication, antennas, and reliability of electronic products.

XIAOBING GAO is currently pursing the master's degree in electronics and communication engineering with Shenzhen University, Shenzhen, China. His research interests include base station antennas and radio frequency.

LONG ZHANG (Member, IEEE) received the B.S. and M.S. degrees in electrical engineering from the Huazhong University of Science and Technology, Wuhan, China, in 2009 and 2012, respectively, and the Ph.D. degree in electronic engineering from the University of Kent, Canterbury, U.K, in 2017. From January 2018 to April 2018, he was a Research Fellow with the Poly-Grames Research Center, Poly technique Montreal, Montreal, QC, Canada. He is currently an Assistant Professor with the College of Electronics and Information Engineering, Shenzhen University, Shenzhen, China. His current research interests include circularly polarized antennas and arrays, mm-wave antennas and arrays, tightly coupled arrays, reflectarrays, and characteristic mode theory. He is a reviewer for several technique journals, including IEEE TRANSACTIONS ON ANTENNAS AND PROPAGATION and IEEE ANTENNAS AND WIRELESS PROPAGATION LETTERS. He was the TPC member and the session chair for several international conferences.

ZHI ZENG (Member, IEEE) received B.S., M.S., and Ph.D. degrees from the Harbin Institute of Technology in 2004, 2006, and 2015, respectively. He was the Vice President of the MOBI Antenna Technology (Shenzhen) Company Ltd., China. He is the Vice Dean of Central Research Institute, Sunway Communication Company Ltd., Shenzhen, China. His research interests include mobile communications, antennas, and radio frequency.